NANO LETTERS

Letter

pubs.acs.org/NanoLett

Pronounced Linewidth Narrowing of an Aluminum Nanoparticle Plasmon Resonance by Interaction with an Aluminum Metallic Film

Ali Sobhani,[†,‡] Alejandro Manjavacas,[§] Yang Cao,[‡,∥] Michael J. McClain,[‡,⊥] F. Javier García de Abajo,[#,▽] Peter Nordlander,[‡,∥] and Naomi J. Halas*[,†,‡,∥]

[†]Department of Electrical and Computer Engineering and [‡]Laboratory for Nanophotonics (LANP), Rice University, Houston, Texas 77005, United States

[§]Department of Physics and Astronomy, University of New Mexico, Albuquerque, New Mexico 87131, United States

[∥]Department of Physics and Astronomy and [⊥]Department of Chemistry, Rice University, Houston, Texas 77005, United States

[#]ICFO - Institut de Ciencies Fotoniques, The Barcelona Institute of Science and Technology, 08860 Castelldefels (Barcelona), Spain

[▽]ICREA - Institució Catalana de Recerca i Estudis Avançats, Barcelona, Spain

Supporting Information

ABSTRACT: Aluminum nanocrystals and fabricated nanostructures are emerging as highly promising building blocks for plasmonics in the visible region of the spectrum. Even at the individual nanocrystal level, however, the localized plasmons supported by Al nanostructures possess a surprisingly broad spectral response. We have observed that when an Al nanocrystal is coupled to an underlying Al film, its dipolar plasmon resonance linewidth narrows remarkably and shows an enhanced scattering efficiency. This behavior is observable in other plasmonic metals, such as gold; however, it is far more dramatic in the aluminum nanoparticle−film system, reducing the dipolar plasmon linewidth by more than half. A substrate-mediated hybridization of the dipolar and quadrupolar plasmons of the nanoparticle reduces the radiative losses of the dipolar plasmon. While this is a general effect that applies to all metallic nanoparticle−film systems, this finding specifically provides a new mechanism for narrowing plasmon resonances in aluminum-based systems, quite possibly expanding the potential of Al-based plasmonics in real-world applications.

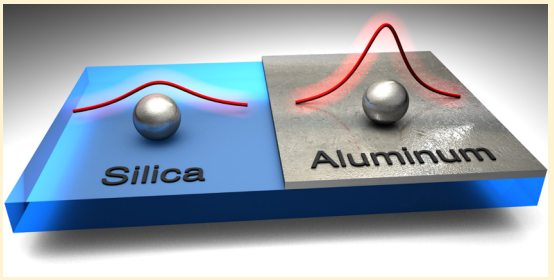

KEYWORDS: *Aluminum, plasmons, nanoparticle, film, radiative losses*

Metallic nanostructures support coherent oscillations of electrons.[1] These excitations, known as surface plasmons,[2] couple strongly to light, concentrating it to subwavelength volumes[3] and producing large optical field enhancements.[4,5] The extraordinary properties of surface plasmons have triggered the development of numerous applications in areas as diverse as nonlinear optics,[6−8] ultrasensitive biosensing,[9−11] photocatalysis,[12,13] and solar energy harvesting.[14,15] However, the majority of these have involved the use of nanostructures made of gold or silver, whose scarcity and resultant high cost clearly limit their large-scale use. Additionally, the intrinsic properties of gold and silver add further constraints; for example, interband transitions in gold (silver) increase the plasmon damping for wavelengths shorter than 550 nm (400 nm), precluding access to much of the visible and UV spectral regions. In addition, the oxidation of silver nanostructures severely degrades the plasmonic response over time, limiting long-term device applications.

Aluminum has recently emerged as a highly viable potential alternative to noble metals for large-scale or large-area plasmonic applications.[16−20] Aluminum nanostructures can support plasmons with wavelengths ranging from the near-IR to the UV, thanks to the high plasma frequency of the bulk material[21−23] and the self-terminating oxide layer that provides long-term stability.[19] Unlike gold and silver, aluminum is compatible with complementary metal-oxide semiconductor (CMOS) technology, opening up new possibilities for integration with electronics in on-chip device applications. Some of these properties have already been used in applications such as nonlinear plasmonics,[24] color filtering,[25−27] or color printing.[28−30] However, to fully exploit the advantages of aluminum for plasmonics, we also need to acknowledge its inherent limitations. One limitation is the broad linewidth of aluminum plasmons at visible frequencies. This broadening is due to an unoccupied band above the Fermi energy that results in interband transitions in the red region of the visible spectrum. So despite improvements in nanofabrication,[31,32] including the recent synthesis of high purity aluminum nanocrystals,[33] the bright plasmon modes of this material are inherently broader than the plasmons supported by noble metal structures due to their larger radiative losses.[34]

Received: July 21, 2015
Revised: September 16, 2015
Published: September 18, 2015

DOI: 10.1021/acs.nanolett.5b02883
Nano Lett. 2015, 15, 6946−6951

Here we report the surprising observation that when aluminum nanocrystals are deposited onto an aluminum film, their dipolar plasmon linewidth is substantially narrowed, which in the case of our experiments, by nominally a factor of 2. In general, it is well-known that the interaction between the nanoparticle and a substrate can alter the optical response of a nanoparticle.[35−37] Substrate-induced modifications are particularly strong for metallic substrates supporting surface plasmon polaritons.[38−43] Here, by carefully monitoring the scattering spectra of individual nanocrystals, we observe that nanoparticles positioned on an aluminum film display a dipolar resonance with a significantly reduced linewidth and enhanced intensity compared with corresponding nanoparticles deposited on a dielectric (silica) substrate. Through a simple theoretical model, we show that the narrowing originates from a substrate-mediated hybridization of the dipolar and quadrupolar nanoparticle plasmons. This interaction reduces the radiative losses of the nanoparticle.

The system we studied is depicted schematically in Figure 1a. It consists of a chemically synthesized aluminum nanocrystal[33]

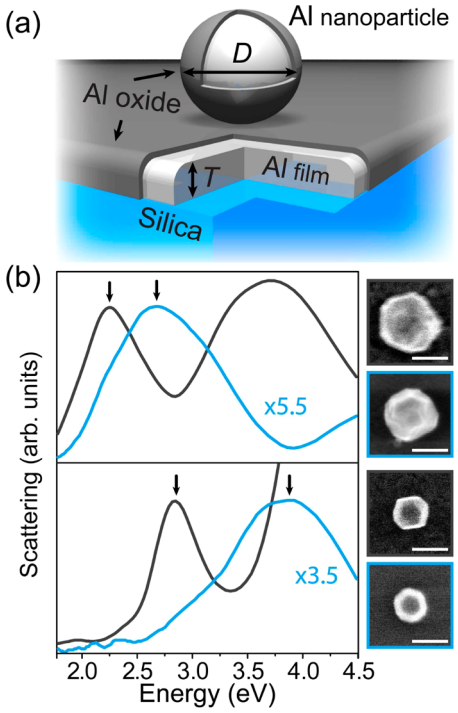

Figure 1. Narrowing of the dipolar plasmon resonance of an aluminum nanoparticle placed on an aluminum film. (a) Schematic of the geometry. (b) Experimentally measured single-particle dark-field scattering spectra of aluminum nanoparticles with diameters D = 180 nm (top) and D = 100 nm (bottom) on an aluminum film of thickness T = 35 nm (gray curves), and directly on the silica substrate (blue curves). Unpolarized illumination and a collection numerical aperture of 0.28 were used in all cases. Right: SEM images of the nanoparticles used to obtain these spectra with the scale bar corresponding to 100 nm.

on an aluminum film of known thickness deposited onto a silica substrate (see Supporting Information for details of the fabrication process). Both the nanocrystal and the film are coated with a self-terminating aluminum oxide layer of a thickness of ∼3 nm that protects each structure from further oxidation.[33] The thickness of the oxide layer is included in the dimensions of both the nanocrystal and the film. We examined the optical response of this coupled system by measuring single-particle scattering spectra in a dark-field microscope using unpolarized illumination (see the Supporting Information for more details on the experimental setup). The corresponding spectra are shown in Figure 1b for Al nanocrystals with diameters of 180 nm (top) and 100 nm (bottom). The spectra shown in gray correspond to a nanocrystal atop an aluminum film of 35 nm thickness, while the blue spectra correspond to a nanocrystal of the same dimension placed directly on the silica substrate. Scanning electron microscope (SEM) images of the analyzed nanocrystals are shown in insets on the right of the figure. For nanocrystals on a silica substrate, both spectra display a single broad peak in this energy range, corresponding to the dipolar plasmon of the nanocrystal. For a nanocrystal on an aluminum film, however, two distinct peaks appear in each scattering spectrum. These can be classified as the hybridized dipolar (lower energy) and quadrupolar (higher energy) modes of the coupled nanocrystal-film system. In all cases, the nature of the modes is identified by analyzing both the corresponding induced charge density maps and the contribution of the different multipolar orders to the scattering spectrum (see Figures S1 and S2 in the Supporting Information for more details). Here, we clearly see that the presence of the aluminum film results in a drastic reduction of the resonance linewidth of the dipolar plasmon mode. For the case of a 180 nm particle diameter, the linewidth (full width at half-maximum, fwhm) is reduced from 1.27 to 0.66 eV, a 48% reduction in linewidth, and for the 100 nm diameter case the linewidth is reduced from 1.38 to 0.48 eV, a 65% reduction in linewidth. This linewidth narrowing is accompanied by a large increase in scattering intensity. This effect appears to be general to plasmonic nanoparticle−film systems but has not been the focus of analysis until now; in ref 44, for example, the linewidth narrowing for a 60 nm diameter gold nanoparticle atop a 30 nm thick gold film is 33%.

To understand the origin of this resonance narrowing, we performed calculations of the scattering efficiency under the same conditions as in the experiment (i.e., unpolarized illumination with the same incident and collection angles). We assume the nanocrystalline particles to be perfectly spherical. The presence of the oxide layer in both the nanocrystal and the film imposes a minimum distance of 6 nm between their metal surfaces, ensuring that nonlocal and quantum effects can be safely neglected.[45−47] This allows us to rely on a classical description based on the solution of Maxwell's equations. We use a semianalytical model[48] that is based on an expansion of the fields into spherical waves centered around the nanoparticle, combined with Mie theory and Fresnel coefficients to describe the response of the nanoparticle and the substrate, respectively. With this approach, we obtain a set of self-consistent equations for the fields that account for the infinite sequence of scattering events between the nanoparticle and the substrate. Upon solving these equations, we obtain the near and far fields, and from them the scattering efficiency (further details on this approach can be found in the Supporting Information.)

Using this semianalytical model, we calculate the scattering efficiency for a nanoparticle of diameter D = 80 nm placed at varying distances H from an aluminum film of thickness T = 35 nm (Figure 2). When the nanoparticle is far from the film, corresponding to when the coupling is weak, the spectrum shows a single broad dipolar resonance. However, when H is reduced and the coupling becomes stronger, the dipolar mode

DOI: 10.1021/acs.nanolett.5b02883
Nano Lett. 2015, 15, 6946−6951

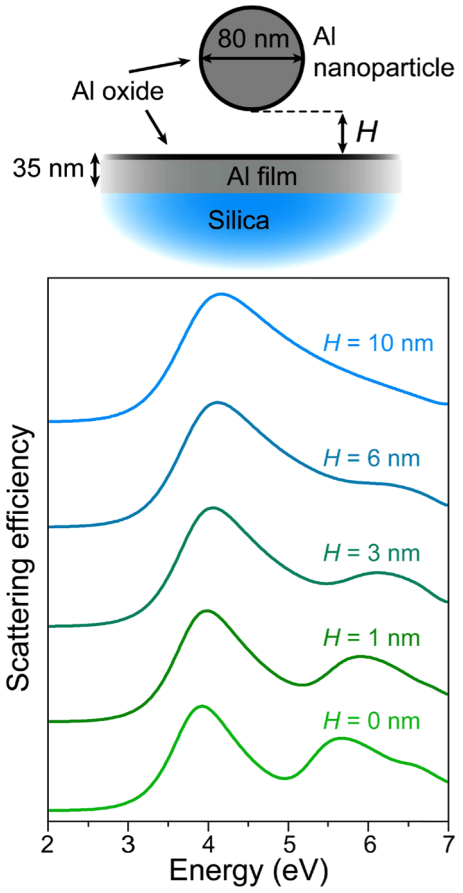

Figure 2. Interaction between an aluminum nanoparticle and an aluminum film. The scheme at the top depicts the geometry used in the calculation. The lower plot shows the scattering efficiency spectrum for a spherical aluminum nanoparticle of diameter D = 80 nm located at a distance H from an aluminum film of thickness T = 35 nm, calculated with the semianalytical model described in the text. We consider unpolarized illumination with the same incident and collection angles as in the experiment.

redshifts slightly and becomes narrower. At the same time, a second resonance, corresponding to the quadrupolar plasmon of the nanoparticle, appears at higher energies. This behavior originates in the hybridization of the dipolar and quadrupolar plasmons of the nanoparticle caused by the symmetry-breaking introduced by the presence of the aluminum substrate. As a result, the quadrupolar resonance acquires part of the "bright" character of the dipolar mode[49,50] becoming easily visible on the scattering spectrum. Correspondingly, the dipolar resonance becomes darker with a reduction in linewidth. Interestingly, mode hybridization has been also exploited in other systems, such as metal−insulator−metal structures, to obtain narrow resonances by reducing the penetration of the electric filed into the metallic parts of the structures.[51]

The scattering efficiency of the dipolar resonance of a nanoparticle is proportional to the square of the amplitude of its polarizability. We can describe the various contributions to this quantity using a straightforward harmonic oscillator model. Within this simple approach, the plasmon is modeled as an oscillator with a total charge q and mass m, whose amplitude satisfies the following equation of motion[52−54]

$$m\ddot{x} = qE - m\omega_0^2 x - m\gamma_{nr}\dot{x} + \frac{2}{3c^3}q^2\dddot{x} \quad (1)$$

The terms on the right-hand side of this expression correspond, respectively, to the driving force associated with the external field $E = E_0 e^{-i\omega t}$, the restoring force with resonant frequency ω_0, the friction caused by the intrinsic damping γ_{nr}, and the Abraham-Lorentz force accounting for the radiation reaction.[55] By solving this equation, we obtain the plasmon dipole moment $d = qx$ and the corresponding well-known expression for the polarizability[56] $\alpha = d/E$

$$\alpha = \frac{\left(\frac{3c^3}{2\omega_0^2}\right)\gamma_r}{\omega_0^2 - \omega^2 - i\gamma_{nr}\omega - i\left(\frac{\omega^3}{\omega_0^2}\right)\gamma_r} \quad (2)$$

Here, we have defined $\gamma_r = (2\omega_0^2/3c^3)(q^2/m)$ as the effective radiative decay rate of the plasmon resonance. The linewidth of the resonance expressed by this polarizability has two contributions, associated with nonradiative losses at a rate γ_{nr} and radiative losses at a rate γ_r. The magnitude of the nonradiative loss is determined by the value of γ_{nr}, which in the absence of finite size effects depends solely on the material properties. The radiative losses, however, are proportional to γ_r. This parameter determines the coupling between the plasmon and the external field and is thus related to the brightness of the resonance (e.g., a completely dark plasmon would have $\gamma_r = 0$). By the dipolar and the quadrupolar modes of the nanoparticle coupling to the aluminum film, the value of γ_r is decreased, which reduces the radiative losses, narrowing the dipolar resonance linewidth. Incidentally, in our experiments the aluminum oxide layer separating the nanocrystal and the film helps prevent an increase in nonradiative losses.

This narrowing mechanism is only efficient for systems in which the radiative losses dominate the linewidth. Because these types of losses occur at a rate γ_r, we expect the narrowing of the linewidth to be more pronounced for nanoparticles with large sizes relative to the wavelength or for those made of materials with a higher plasma frequency. This explains why linewidth narrowing is a smaller effect for gold. To corroborate this hypothesis, we use the semianalytical model to calculate the scattering spectrum of spherical aluminum nanoparticles with different diameters. Figure 3a shows the spectra obtained for aluminum nanoparticles of increasing diameter on an aluminum film with T = 35 nm (left panel), as well as for the same nanoparticles sitting directly on a silica substrate (right panel). Comparing these spectra we observe that, for all values of D under consideration, the dipolar resonance is narrower when the nanoparticles are on the aluminum film. However, the difference in linewidth between dielectric and metallic film substrates varies with particle diameter. This is shown in Figure 3b, where we plot the linewidth as a function of particle diameter obtained by fitting the dipolar resonances of Figure 3a to Lorentzian functions, both for the nanoparticles on the aluminum film (gray) and on the silica substrate (blue). Interestingly, the linewidth for the nanoparticles placed on the aluminum film remains almost constant, suggesting that radiative losses are already substantially reduced by the presence of the film. For the nanoparticles on a dielectric substrate (silica), the linewidth seems to reach a saturation value, likely due to both the nonlinear dependence between γ_r and D, and the redshift of the resonance. Similar calculations using nanoparticles and films made of gold instead of aluminum are shown in Figure S3 of the Supporting Information, showing that, as expected, the narrowing of the resonance is less efficient than in the aluminum structures due to the lower frequencies of

DOI: 10.1021/acs.nanolett.5b02883
Nano Lett. 2015, 15, 6946−6951

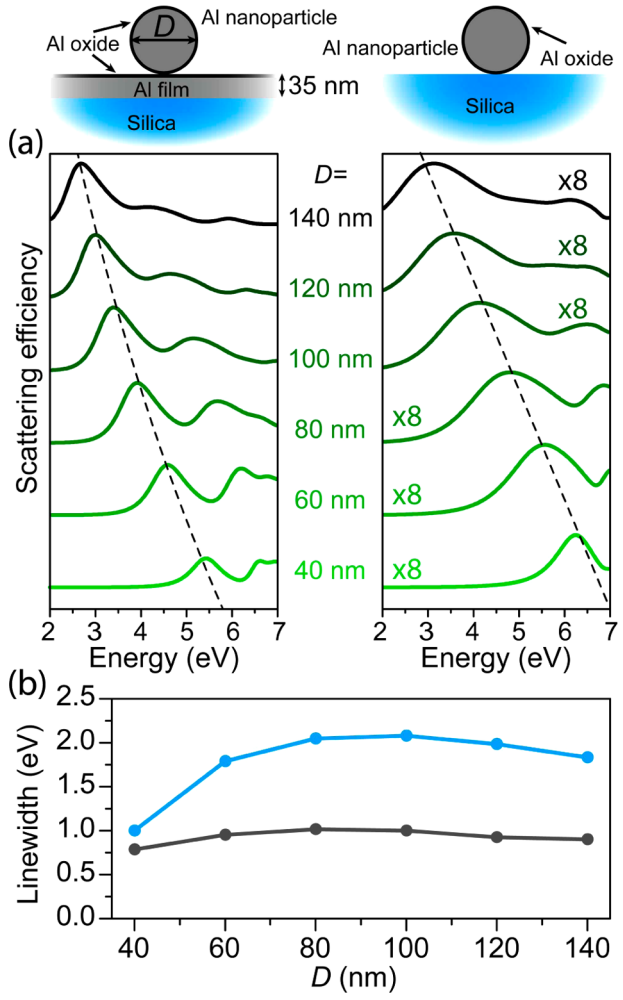

Figure 3. Effect of nanoparticle size on the narrowing of the plasmon resonance linewidth. (a) Calculated scattering efficiency spectra for aluminum nanoparticles of different diameters D placed on a T = 35 nm aluminum film (left) and on a silica substrate (right). The spectra in the right panel are multiplied by a factor of 8 to improve visibility. The dashed lines serve as a guide for the eye to indicate the trend of the dipolar resonance. The upper insets show the schematics of the simulated geometries. All calculations are performed using the same method and conditions as in Figure 2. (b) Calculated linewidth of the dipolar resonance for the nanoparticles on the aluminum film (gray) and on the silica substrate (blue), as obtained from the spectra of panel (a).

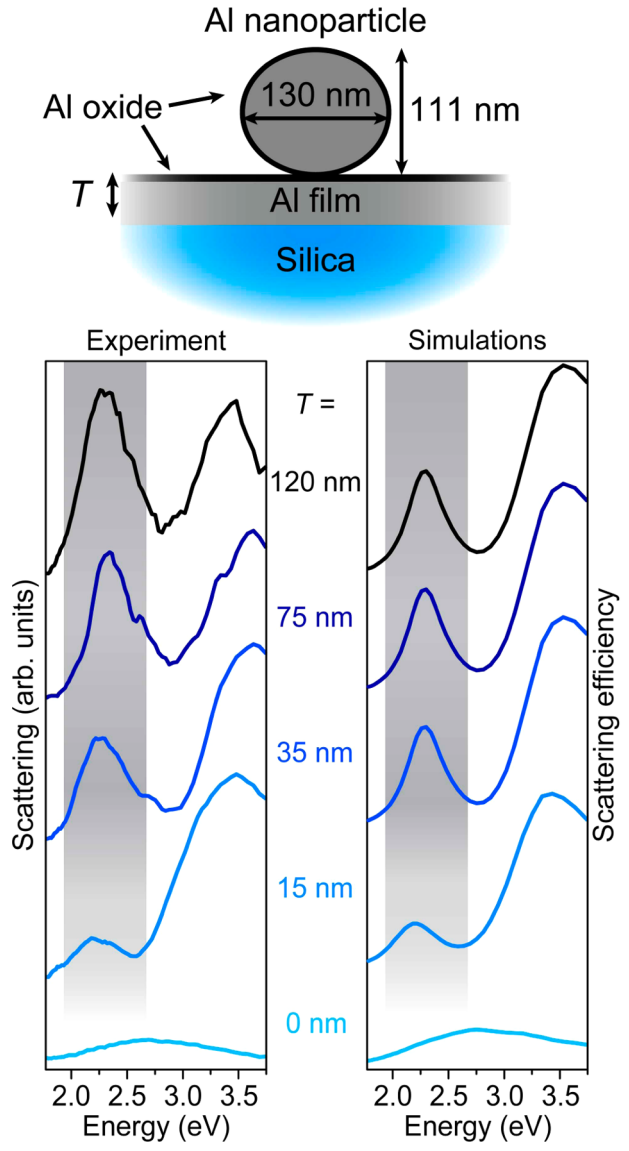

Figure 4. Effect of film thickness on the plasmon linewidth. The left panel shows a series of experimental single-particle scattering spectra for aluminum nanoparticles of diameter D = 130 nm placed on top of aluminum films of different thicknesses T, as depicted in the upper inset. The right panel shows numerical simulations of the scattering efficiency performed by using a finite-difference time-domain approach for the same film thicknesses shown in the left panel. In both panels the case with T = 0 refers to the particle positioned directly on the silica substrate.

the gold dipolar plasmon. Although the narrowing is associated with the darkening of the dipolar plasmon, the scattering efficiency for the nanoparticles on the aluminum film is almost 1 order of magnitude larger than for nanoparticles of the same dimension on a silica substrate, as shown both experimentally in Figure 1b and theoretically in Figure 3a. This is because the field exciting the nanoparticle contains a component coming from the reflection on the substrate, which is obviously larger when the aluminum film is present. The same effect causes an enhancement of the scattered intensity by redirecting the light emitted toward the substrate. Therefore, the coupling with the aluminum film produces not only narrower but also brighter resonances.

To further characterize the plasmon narrowing mechanism, we measure the single-particle scattering spectra of aluminum nanocrystals of D = 130 nm deposited on aluminum films with varying thicknesses T. The experimental spectra are shown in the left panel of Figure 4. For values of T larger than 35 nm, the linewidth of the dipolar resonance (signaled by a shadowed area) remains almost constant. However, when the thickness of the aluminum film decreases, becoming comparable to the skin depth of the material (~15 nm for aluminum at 2.3 eV), the dipolar plasmon peak height is reduced and broadens, approaching the case of no aluminum film (i.e., T = 0). These experimental results are well supported by the numerical calculations shown in the right panel, which are obtained by solving Maxwell's equations using the finite-difference time-domain method (see the Supporting Information for more details). We use this approach instead of the semianalytical

DOI: 10.1021/acs.nanolett.5b02883
Nano Lett. 2015, 15, 6946−6951

model because it allows us to introduce the nonspherical shape of the nanoparticles. This is necessary because the Al nanocrystals used in the experiment are not completely spherical (Figure 1b), so we model them as ellipsoids (see sketch in the upper part of Figure 4) with a surface-parallel long axis of 130 nm and a perpendicular short axis of 111 nm. We use the same unpolarized illumination, incident direction, and collection angles as in the experiment. The very close agreement between experiment and simulation further supports our interpretation of the narrowing mechanism.

In summary, we have shown that the coupling of an aluminum nanoparticle to an underlying aluminum film results in dipolar plasmon resonances with significantly reduced linewidths and enhanced intensity compared with an aluminum nanoparticle placed on a dielectric substrate. We show that this effect is due to a reduction in the radiative losses of the dipolar plasmon, which is caused by the substrate-mediated hybridization of this mode with the quadrupolar mode of the nanoparticle. The narrowing mechanism described in this work is expected to happen for any metal, although is larger for systems whose dissipation is dominated by radiative losses, as is the case with aluminum, due to its higher plasma frequency relative to silver or gold. We also address the dependence of this linewidth narrowing effect on particle diameter, and on film thickness. While general, the results presented here describe a new and specific mechanism for reducing the scattering linewidth of aluminum nanostructures. Indeed, these observations may substantially influence future aluminum plasmonic nanostructure design to exploit film-coupling effects in line shape-engineered devices from which applications requiring narrow resonances could benefit.

■ ASSOCIATED CONTENT

Supporting Information

The Supporting Information is available free of charge on the ACS Publications website at DOI: 10.1021/acs.nanolett.5b02883.

Detailed descriptions of the sample fabrication, the experimental setup, and the theoretical methods. Also, a detailed analysis of the character of the different modes showing up on the scattering spectra, the decomposition of the latter on the contributions associated with the different multipolar orders, and results equivalent to those of Figure 3b for the case of gold nanoparticles on gold films. (PDF)

■ AUTHOR INFORMATION

Corresponding Author

*E-mail: halas@rice.edu.

Author Contributions

A.S. and A.M. contributed equally to this paper.

Notes

The authors declare no competing financial interest.

■ ACKNOWLEDGMENTS

A.M. acknowledges financial support from the Welch foundation through the J. Evans Attwell-Welch Postdoctoral Fellowship Program of the Smalley Institute of Rice University and the Department of Physics and Astronomy and the College of Arts and Sciences of the University of New Mexico. N.J.H and P.N acknowledge support from the Robert A. Welch Foundation under Grants C-1220 and C-1222 and the Army Research Office under Grant W911NF-12-1-0407. F.J.G.deA. acknowledges support from the Spanish Mineco (Grant MAT2014-59096-P).

■ REFERENCES

(1) Novotny, L.; Hecht, B. *Principles of Nano-Optics*; Cambridge University Press: New York, 2006.
(2) Maier, S. A. *Plasmonics: Fundamentals and Applications*; Springer: New York, 2007.
(3) Álvarez-Puebla, R. A.; Liz-Marzán, L. M.; García de Abajo, F. J. *J. Phys. Chem. Lett.* **2010**, *1*, 2428−2434.
(4) Oulton, R. F.; Sorger, V. J.; Zentgraf, T.; Ma, R. M.; Gladden, C.; Dai, L.; Bartal, G.; Zhang, X. *Nature* **2009**, *461*, 629−632.
(5) Akselrod, G. M.; Argyropoulos, C.; Hoang, T. B.; Ciracì, C.; Fang, C.; Huang, J.; Smith, D. R.; Mikkelsen, M. H. *Nat. Photonics* **2014**, *8*, 835−840.
(6) Kim, S.; Jin, J.; Kim, Y.-J.; Park, I.-Y.; Kim, Y.; Kim, S.-W. *Nature* **2008**, *453*, 757−760.
(7) Sivis, M.; Duwe, M.; Abel, B.; Ropers, C. *Nat. Phys.* **2013**, *9*, 304−309.
(8) Lassiter, J. B.; Chen, X.; Liu, X.; Ciracì, C.; Hoang, T. B.; Larouche, S.; Oh, S.-H.; Mikkelsen, M. H.; Smith, D. R. *ACS Photonics* **2014**, *1*, 1212−1217.
(9) Xu, H.; Bjerneld, E. J.; Käll, M.; Börjesson, L. *Phys. Rev. Lett.* **1999**, *83*, 4357−4360.
(10) Anker, J. N.; Hall, W. P.; Lyandres, O.; Shah, N. C.; Zhao, J.; Van Duyne, R. P. *Nat. Mater.* **2008**, *7*, 442−453.
(11) Zhang, R.; Zhang, Y.; Dong, Z. C.; Jiang, S.; Zhang, C.; Chen, L. G.; Zhang, L.; Liao, Y.; Aizpurua, J.; Luo, Y.; Yang, J. L.; Hou, J. G. *Nature* **2013**, *498*, 82−86.
(12) Liu, Z.; Hou, W.; Pavaskar, P.; Aykol, M.; Cronin, S. B. *Nano Lett.* **2011**, *11*, 1111−1116.
(13) Clavero, C. *Nat. Photonics* **2014**, *8*, 95−103.
(14) Catchpole, K. R.; Polman, A. *Opt. Express* **2008**, *16*, 21793−21800.
(15) Atwater, H. A.; Polman, A. *Nat. Mater.* **2010**, *9*, 205−213.
(16) Langhammer, C.; Schwind, M.; Kasemo, B.; Zorić, I. *Nano Lett.* **2008**, *8*, 1461−1471.
(17) Chan, G. H.; Zhao, J.; Schatz, G. C.; Duyne, R. P. V. *J. Phys. Chem. C* **2008**, *112*, 13958−13963.
(18) Ekinci, Y.; Solak, H. H.; Löfler, J. F. *J. Appl. Phys.* **2008**, *104*, 083107.
(19) Knight, M. W.; King, N. S.; Liu, L.; Everitt, H. O.; Nordlander, P.; Halas, N. J. *ACS Nano* **2014**, *8*, 834−840.
(20) Gérard, D.; Gray, S. K. *J. Phys. D: Appl. Phys.* **2015**, *48*, 184001.
(21) Ekinci, Y.; Solak, H. H.; David, C. *Opt. Lett.* **2007**, *32*, 172−174.
(22) Maidecchi, G.; Gonella, G.; Proietti Zaccaria, R.; Moroni, R.; Anghinolfi, L.; Giglia, A.; Nannarone, S.; Mattera, L.; Dai, H.-L.; Canepa, M.; Bisio, F. *ACS Nano* **2013**, *7*, 5834−5841.
(23) Lecarme, O.; Sun, Q.; Ueno, K.; Misawa, H. *ACS Photonics* **2014**, *1*, 538−546.
(24) Castro-Lopez, M.; Brinks, D.; Sapienza, R.; van Hulst, N. F. *Nano Lett.* **2011**, *11*, 4674−4678.
(25) Chen, Q.; Cumming, D. R. S. *Opt. Express* **2010**, *18*, 14056−14062.
(26) Xu, T.; Wu, Y.-K.; Luo, X.; Guo, L. J. *Nat. Commun.* **2010**, *1*, 59.
(27) Inoue, D.; Miura, A.; Nomura, T.; Fujikawa, H.; Sato, K.; Ikeda, N.; Tsuya, D.; Sugimoto, Y.; Koide, Y. *Appl. Phys. Lett.* **2011**, *98*, 093113.
(28) Clausen, J. S.; Højlund-Nielsen, E.; Christiansen, A. B.; Yazdi, S.; Grajower, M.; Taha, H.; Levy, U.; Kristensen, A.; Mortensen, N. A. *Nano Lett.* **2014**, *14*, 4499−4504.
(29) Tan, S. J.; Zhang, L.; Zhu, D.; Goh, X. M.; Wang, Y. M.; Kumar, K.; Qiu, C.-W.; Yang, J. K. W. *Nano Lett.* **2014**, *14*, 4023−4029.
(30) Olson, J.; Manjavacas, A.; Liu, L.; Chang, W.-S.; Foerster, B.; King, N. S.; Knight, M. W.; Nordlander, P.; Halas, N. J.; Link, S. *Proc. Natl. Acad. Sci. U. S. A.* **2014**, *111*, 14348−14353.

DOI: 10.1021/acs.nanolett.5b02883
Nano Lett. 2015, 15, 6946−6951

(31) Diest, K.; Liberman, V.; Lennon, D. M.; Welander, P. B.; Rothschild, M. *Opt. Express* **2013**, *21*, 28638−28650.
(32) Martin, J.; Plain, J. *J. Phys. D: Appl. Phys.* **2015**, *48*, 184002.
(33) McClain, M. J.; Schlather, A. E.; Ringe, E.; King, N. S.; Liu, L.; Manjavacas, A.; Knight, M. W.; Kumar, I.; Whitmire, K. H.; Everitt, H. O.; Nordlander, P.; Halas, N. J. *Nano Lett.* **2015**, *15*, 2751−2755.
(34) Ross, M. B.; Schatz, G. C. *J. Phys. D: Appl. Phys.* **2015**, *48*, 184004.
(35) Knight, M. W.; Wu, Y.; Lassiter, J. B.; Nordlander, P.; Halas, N. J. *Nano Lett.* **2009**, *9*, 2188−2192.
(36) Vernon, K. C.; Funston, A. M.; Novo, C.; Gómez, D. E.; Mulvaney, P.; Davis, E. *Nano Lett.* **2010**, *10*, 2080−2086.
(37) Dahan, N.; Greffet, J. J. *Opt. Express* **2012**, *20*, A530−A544.
(38) Lévêque, G.; Martin, O. J. F. *Opt. Express* **2006**, *14*, 9971−9981.
(39) Le, F.; Lwin, N. Z.; Steele, J. M.; Käll, M.; Halas, N. J.; Nordlander, P. *Nano Lett.* **2005**, *5*, 2009−2013.
(40) Mock, J. J.; Hill, R. T.; Degiron, A.; Zauscher, S.; Chilkoti, A.; Smith, D. R. *Nano Lett.* **2008**, *8*, 2245−2252.
(41) Hu, M.; Ghoshal, A.; Marquez, M.; Kik, P. G. *J. Phys. Chem. C* **2010**, *114*, 7509−7514.
(42) Lumdee, C.; Toroghi, S.; Kik, P. G. *ACS Nano* **2012**, *6*, 6301−6307.
(43) Moreau, A.; Ciraci, C.; Mock, J. J.; Hill, R. T.; Wang, Q.; Wiley, B. J.; Chilkoti, A.; Smith, D. R. *Nature* **2012**, *492*, 86−89.
(44) Mock, J. J.; Hill, R. T.; Tsai, Y.-J.; Chilkoti, A.; Smith, D. R. *Nano Lett.* **2012**, *12*, 1757−1764.
(45) García de Abajo, F. J. *J. Phys. Chem. C* **2008**, *112*, 17983−17987.
(46) Ciracì, C.; Hill, R. T.; Mock, J. J.; Urzhumov, Y.; Fernández-Domínguez, A. I.; Maier, S. A.; Pendry, J. B.; Chilkoti, A.; Smith, D. R. *Science* **2012**, *337*, 1072−1074.
(47) Raza, S.; Bozhevolnyi, S. I.; Wubs, M.; Mortensen, N. A. *J. Phys.: Condens. Matter* **2015**, *27*, 183204.
(48) Kühler, P.; García de Abajo, F. J.; Leiprecht, P.; Kolloch, A.; Solis, J.; Leiderer, P.; Siegel, J. *Opt. Express* **2012**, *20*, 22063−22078.
(49) Nordlander, P.; Prodan, E. *Nano Lett.* **2004**, *4*, 2209−2213.
(50) Chu, M. W.; Myroshnychenko, V.; Chen, C. H.; Deng, J. P.; Mou, C. Y.; García de Abajo, F. J. *Nano Lett.* **2009**, *9*, 399−404.
(51) Berini, P. *Adv. Opt. Photonics* **2009**, *1*, 484−588.
(52) Kats, M. A.; Yu, N.; Genevet, P.; Gaburro, Z.; Capasso, F. *Opt. Express* **2011**, *19*, 21748−21753.
(53) Asenjo-Garcia, A.; Manjavacas, A.; García de Abajo, F. J. *Phys. Rev. Lett.* **2011**, *106*, 213601.
(54) Li, Y.; Zhao, K.; Sobhani, H.; Bao, K.; Nordlander, P. *J. Phys. Chem. Lett.* **2013**, *4*, 1352−1357.
(55) Jackson, J. D. *Classical Electrodynamics*; Wiley: New York, 1975.
(56) Carminati, R.; Greffet, J. J.; Henkel, C.; Vigoreaux, J. M. *Opt. Commun.* **2006**, *261*, 368−375.

DOI: 10.1021/acs.nanolett.5b02883
Nano Lett. 2015, 15, 6946−6951

Pronounced Linewidth Narrowing of an Aluminum Nanoparticle Plasmon Resonance by Interaction with an Aluminum Metallic Film

Ali Sobhani,[†,‡,#] Alejandro Manjavacas,[¶,#] Yang Cao,[§,‡] Michael J. McClain,[‖,‡] F. J. García de Abajo,[⊥] Peter Nordlander,[§,‡] and Naomi J. Halas[*,§,†,‡]

†*Department of Electrical and Computer Engineering, Rice University, Houston, Texas, United States*

‡*Laboratory for Nanophotonics (LANP), Rice University, Houston, Texas, United States*

¶*Department of Physics and Astronomy, University of New Mexico, Albuquerque, New Mexico, United States*

§*Department of Physics and Astronomy, Rice University, Houston, Texas, United States*

‖*Department of Chemistry, Rice University, Houston, Texas, United States*

⊥*ICFO - Institut de Ciencies Fotoniques, The Barcelona Institute of Science and Technology, 08860 Castelldefels (Barcelona), Spain and ICREA - Institució Catalana de Recerca i Estudis Avançats, Barcelona, Spain*

#*Contributed equally to this work*

E-mail: halas@rice.edu

Sample fabrication

The silica substrates were first cleaned by sonicating them in acetone for 5 min and rinsed with isopropyl alcohol. After that, the substrates were masked with alignment grids used for transmission electron microscopy, and then 99.999% pure aluminum was evaporated over them with the desired thickness. The base pressure of the chamber and the evaporation rate were 5×10^{-7} Torr and 1 Å/s, respectively. The aluminum nanocrystals were deposited on the substrate by diluting them in isopropanol alcohol (concentration) and then spin coating the solution on the substrate (1500 rpm, 1 min).

Experimental setup

The samples were illuminated using a continuum light source (Energetiq LDLS) filtered with a monochromator. The illumination was focused on the substrate with an incidence angle of 50º, using reflective optics to minimize the optical losses along the beam path. The dark-field scattering signal of the particles was collected at normal angle using a 15x, 0.28 NA finite conjugate objective (Edmund Optics, UV ReflX).

Theoretical methods

Semianalytical model

The semianalytical model used in this work was developed in Ref. 1. In brief, the method starts with an expansion of all fields in terms of spherical waves centered on the nanoparticle. Then Mie theory is used to relate the fields scattered by the nanoparticle with the corresponding incident fields. Similarly, Fresnel coefficients are used to calculate the fields reflected and transmitted by the substrate. Conversion matrices between spherical and plane waves in the particle-substrate gap are introduced to switch between the two representations in that region, thus allowing us to plug Mie coefficients to describe scattering by the former and Fresnel coefficients for the latter. Imposing the adequate continuity conditions to the

fields, a self-consistent set of equations is obtained, which accounts for the series of infinite scattering and reflection events happening at the nanoparticle and the substrate, respectively. Solving these equations, the electric field, and therefore, the scattering intensity are obtained. We used similar conditions as in the experimental setup, corresponding to incident and collection angles of 50° and 16°, respectively. We also assumed a 3 nm thick aluminum oxide layer covering both the nanoparticles and the film. The dielectric functions of aluminum, aluminum oxide, and silica were taken from Ref. 2.

Numerical simulations

We performed numerical simulations for Figure 4 of the main paper using a commercial finite-difference time-domain (FDTD) software package (Lumerical 8.9.163). The shape and size of the nanoparticles were chosen based on the experimental scanning electron microscope (SEM) images. In all cases the nanoparticles and the aluminum films were covered with a 3 nm thick aluminum oxide layer. Unless otherwise stated, we used unpolarized illumination, with an incidence angle of 50° and a collection angle of 16° with respect to the substrate normal, in accordance with the experimental conditions. As in the semianalytical model, the dielectric functions of aluminum, aluminum oxide, and silica were taken from Ref. 2. Perfect-matched layers were used as boundary conditions to simulate the infinite substrate and absorb scattered light. All calculations were converged to ensure the reliability and accuracy of the simulation results.

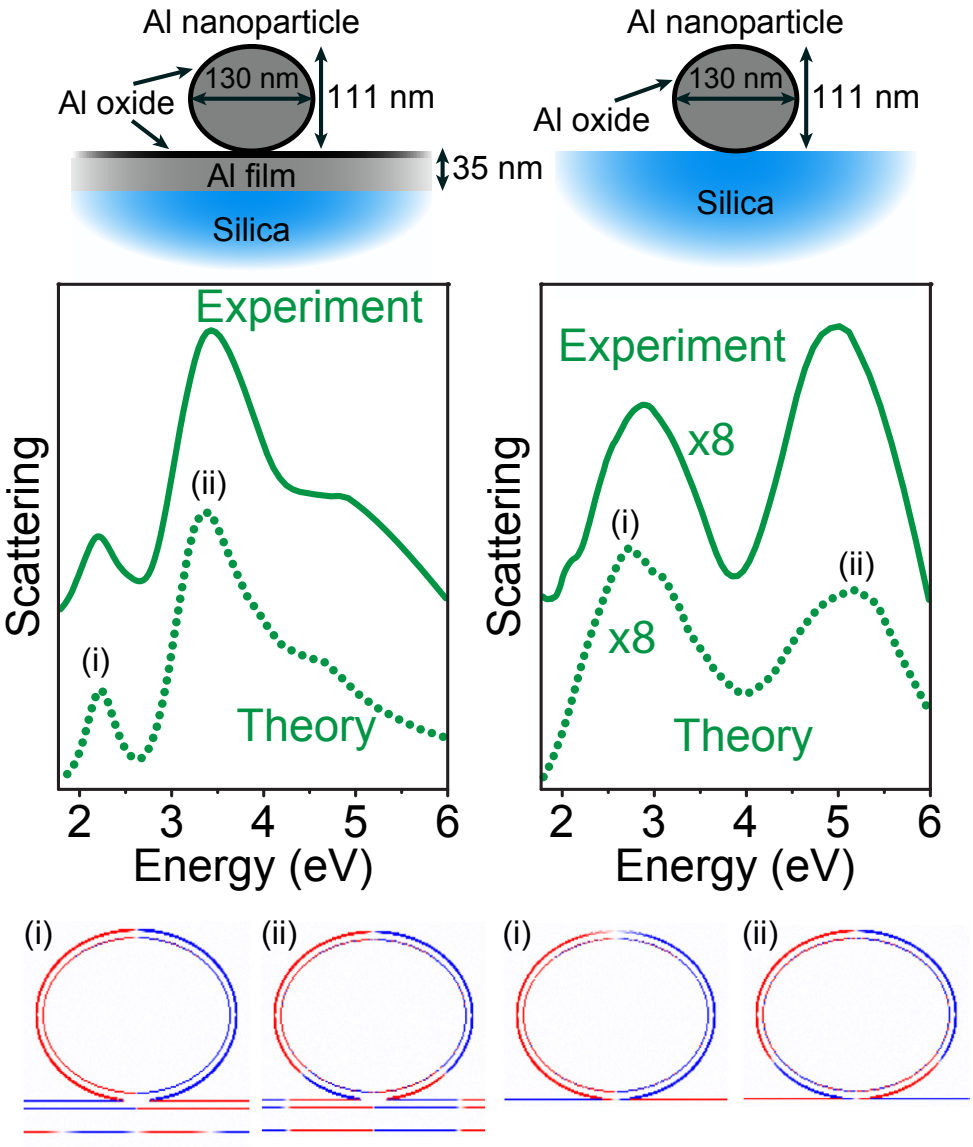

Figure 1: Analysis of the character of the different modes appearing on the scattering spectra. We compare the experimental spectra with numerical simulations performed using a FDTD solver (see previous section). The corresponding results are shown in the middle panel, for the nanoparticle sitting either on the aluminum film (left) or the silica substrate (right). The agreement between experiment and theory is remarkable. The different geometrical parameters used in the simulations are shown in the upper panels. For simplicity, we consider s-polarized illumination in both the experimental and the simulated spectra. Furthermore, to improve visibility, the experimental spectra are vertically offset, and all curves in the right plot are multiplied by a factor of 8. Analyzing the induced charge densities of the different resonances, we confirm that the first peak of these spectra (i) corresponds to a dipolar mode, while the second one (ii) is associated with a quadrupolar mode.

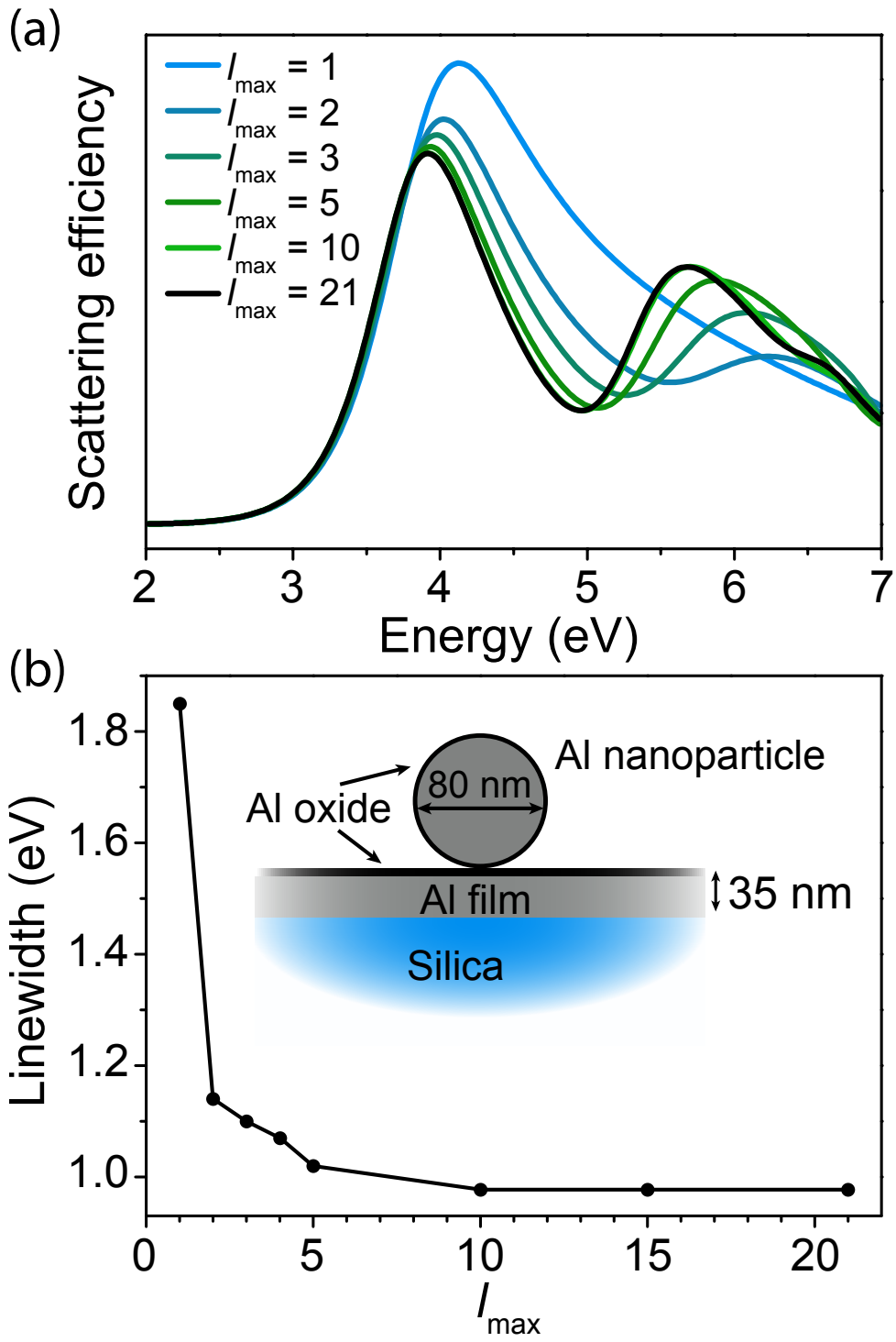

Figure 2: Analysis of the contribution of the different multipolar orders to the nanoparticle scattering. (a) Scattering efficiency calculated for different cutoffs on the multipolar expansion, l_{max}. We consider a spherical aluminum nanoparticle of diameter $D = 80\,\text{nm}$ located on an aluminum film of thickness $T = 35\,\text{nm}$ (see inset on panel (b), notice that the particle and the film are separated by two 3 nm-thick oxide layers). (b) Calculated linewidth of the dipolar resonance as a function of l_{max}.

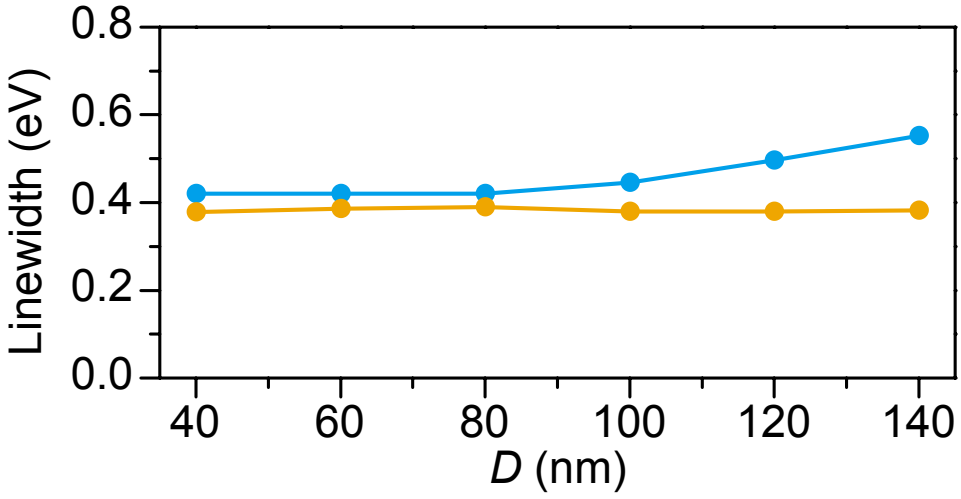

Figure 3: Comparison of the linewidth of the dipolar resonance of gold nanoparticles deposited on gold films and silica substrates. The geometry under consideration is the same as in Figure 3 of the main paper. Namely, nanoparticles with different diameters D are placed 6 nm away from a $T = 35$ nm thick gold film (orange curve) or from the silica substrate (blue curve).

References

(1) Kühler, P.; García de Abajo, F. J.; Leiprecht, P.; Kolloch, A.; Solis, J.; Leiderer, P.; Siegel, J. *Opt. Express* **2012**, *20*, 22063–22078.

(2) Palik, E. D. *Handbook of Optical Constants of Solids*; Academic Press: San Diego, 1985.